

Multichannel field-effect spin barrier selector

G. E. Marques,¹ A. C. R. Bittencourt,² C. F. Destefani,³ and Sergio E. Ulloa³

¹Departamento de Física, Universidade Federal de São Carlos, 13.565-905, São Carlos, São Paulo, Brazil

²Departamento de Física, Universidade Federal do Amazonas, 67.077-000, Manaus, Amazonas, Brazil

³Department of Physics and Astronomy, Ohio University, 45701-2979, Athens, Ohio, USA

(Dated: October 8, 2018)

We have studied spin carrier dynamics under full spin-orbit coupling. The anisotropy of dispersions for independent circular spinor polarizations is explored as a possible vertical multichannel voltage controlled spin-filter. Small voltage variations are found to select the current polarizations in a resonant tunneling geometry.

PACS numbers: 71.70.Ej, 73.21.La, 78.30.Fs

Keywords: spin-orbit coupling, field-effect transistor, spin polarized

The advent of *spintronics* has resulted in the study and design of spin manipulated devices used as information processors, quantum computing elements, spin-polarized diodes, spin-valve read heads,¹ and electro-optical modulators,² to name just a few. The spin-orbit (SO) interaction, due to spatial asymmetry in zincblende lattices or sample design, doping profile or applied gate voltages, plays a fundamental role on these systems,^{3,4} especially on spin-dependent tunnelling. The SO interaction couples the electronic momentum to the spin degrees of freedom, and lifts the spin degeneracy for structures fabricated in zincblende materials. The narrower the energy gap of the host material, the stronger these effects will appear on the transport⁵ and optical properties.⁶

We present here a detailed analysis of the complexity of bulk electronic structure, derived from kinetic energy plus the *full* SO Hamiltonian including Bychkov-Rashba⁷ and *all three* Dresselhaus⁸ contributions. Then, we study SO effects on spin-polarized current in double-barrier resonant (DBR) devices, and analyze how the anisotropy on the spin orientation and polarization of spinor states can be used to *select* and optimize channels for vertical transport in the system.

Recent publications have proposed the manipulation of linear Rashba and Dresselhaus terms in the SO interaction.⁹ The cancellation of *linear* terms leads to drift-diffusive lateral transistors, in contrast to the ballistic operation of the Datta-Das device.² Perel *et al*¹⁰ have also reported on the evolution of the spin orientation with 2D transverse momentum, and explored the tunnelling through a single barrier with different III-V materials, driven only by the linear k_{\parallel} Dresselhaus term. A time-dependent spin manipulation scheme has been recently proposed.¹¹

Let $\sigma = +$ ($-$) label the *spin-up* (*spin-down*) state. The carrier dynamics, driven by the kinetic energy plus *full* SO Hamiltonian, is dictated by

$$\begin{bmatrix} H_{++} & H_{+-} \\ H_{-+} & H_{--} \end{bmatrix} \begin{bmatrix} F_+(z) \\ F_-(z) \end{bmatrix} e^{i\mathbf{k}_{\parallel} \cdot \rho} = E \begin{bmatrix} F_+(z) \\ F_-(z) \end{bmatrix} e^{i\mathbf{k}_{\parallel} \cdot \rho}. \quad (1)$$

In this equation, the diagonal terms are $H_{\sigma\sigma} = -(\hbar^2/2m^*)d^2/dz^2 + (\hbar^2k_{\parallel}^2/2m^*) - i\sigma\alpha_2(k_{\parallel}, \varphi)d/dz$, while

the off-diagonal term is $H_{+-} = \beta_R(k_{\parallel}, \varphi) + \alpha_3(k_{\parallel}, \varphi) + \alpha_1(k_{\parallel}, \varphi)d^2/dz^2$, with $H_{+-} = H_{+-}^{\dagger}$. In this context, $\mathbf{k}_{\parallel} = (k_x, k_y) = (k_{\parallel}, \varphi)$ is the in-plane wave vector, $\rho = (x, y)$ is the electron position in the xy plane, $\alpha_1(k_{\parallel}, \varphi) = \alpha_0 k_{\parallel} e^{i\varphi}$, $\alpha_2(k_{\parallel}, \varphi) = \alpha_0 k_{\parallel}^2 \cos 2\varphi$ and $\alpha_3(k_{\parallel}, \varphi) = \alpha_0 k_{\parallel}^3 (e^{i\varphi} - e^{-i3\varphi})/4$ are, respectively, the linear, quadratic and cubic Dresselhaus SO terms. Finally, $\beta_R(k_{\parallel}, \varphi) = \beta_0(-dV_R/dz)k_{\parallel} e^{i(\pi/2-\varphi)}$ is the linear Bychkov-Rashba contribution under any potential profile $V_R(z)$, whereas $F_{\pm}(z)$ are the spinor components. Here, α_0 and β_0 are the SO material constants.¹²

First let us discuss bulk dispersions where k_z is a good quantum number for the $-id/dz$ operator. Due to the strong coupling between spin s and linear momentum $\mathbf{k} = (\mathbf{k}_{\parallel}, k_z)$ degrees of freedom, the Dresselhaus (or bulk inversion asymmetry, BIA) and Bychkov-Rashba (or surface inversion asymmetry, SIA) Hamiltonians create special sectors and anisotropies on the spinor phase-space. For given \mathbf{k}_{\parallel} and applied electric field $F_0 = -(1/e)dV_R/dz$, the bulk eigenvalues of the full Hamiltonian in Eq. 1 are

$$E_{\pm}(\mathbf{k}_{\parallel}, k_z) = \frac{\hbar^2}{2m^*} (k_{\parallel}^2 + k_z^2) \pm \sqrt{\gamma(\mathbf{k}_{\parallel}, k_z) + \delta(\mathbf{k}_{\parallel})}, \quad (2)$$

where $\gamma(\mathbf{k}_{\parallel}, k_z) = \alpha_0^2 k_{\parallel}^4 k_z^2 \cos(4\varphi) + \alpha_0^2 k_{\parallel}^2 k_z^4 - 2\alpha_0 \beta k_{\parallel}^2 k_z^2 \sin(2\varphi)$ and $\delta(\mathbf{k}_{\parallel}) = \beta^2 k_{\parallel}^2 + \alpha_0^2 k_{\parallel}^6 \sin^2(2\varphi)/4 + \alpha_0 \beta k_{\parallel}^4 \sin(2\varphi)$. Here φ is measured from the $(1, 0)$ crystalline axis on the xy plane and $\beta = \beta_0(-dV_R/dz)$.

Notice that from the four degeneracies, two for the momentum ($\pm k_z$) and two for spin (\pm), one can construct only two independent spinor states forming the Kramers doublet. Without SO, there are two degenerate states, well known as *linear spin polarized*, where the *spin-up* and *spin-down* spinors display isotropic parabolic dispersions for both k_{\parallel} and k_z (first term in Eq. 2). However, with SO there are two orthogonal Hilbert subspaces, the *circular spin polarized* states, with highly anisotropic dispersions when the orbital angle, φ , changes clockwise (σ^+) and counterclockwise (σ^-), respectively. The gap measuring the spin-splitting is $E_g^{\sigma}(k_{\parallel}, \varphi, k_z) = [E_+(k_{\parallel}, \varphi, k_z) - E_-(k_{\parallel}, \varphi, k_z)]$, or twice the square root

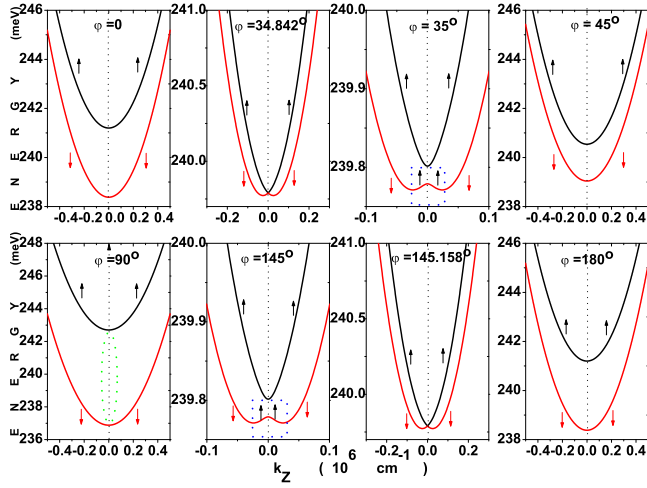


FIG. 1: Angular anisotropies and bulk dispersions for σ^+ -polarization at special angles within the interval $0 \leq \varphi \leq 180^\circ$. Notice spin polarization in different sectors of k_z . Panels at $\varphi = \varphi_c^+ = 34.842^\circ$ and at $\varphi = 145.158^\circ$ show no spin gap.

in Eq. 2. At $k_z = 0$, this yields a critical angle $\varphi_c^\sigma = -0.5 \sin^{-1}[-2\beta/(\alpha_0 k_{\parallel}^2)]$ where $E_g^\sigma(k_{\parallel}, \varphi_c^\sigma, k_z) = 0$. This result depends on the field strength and on the ratio between SO constants, and defines a maximum value for k_{\parallel} , given by $k_{\parallel}^c = \sqrt{-2\beta/\alpha_0}$. There are two symmetry regimes according to which SO mechanism is dominant: (a) *SIA regime*, or Rashba dominant, for $k_{\parallel} \leq k_{\parallel}^c$, and (b) *BIA regime*, or Dresselhaus dominant, for $k_{\parallel} > k_{\parallel}^c$. These properties are valid for any zincblende material and here we will fix our attention on InSb, due to its large SO parameters.¹² These states and their properties are reminiscent of circularly-polarized light travelling through a crystal, as we shall discuss later. It is convenient to define a new zero for the angle at the $(1, -1)$ crystalline direction in the xy plane, corresponding to a rotation $\varphi \Rightarrow \varphi - 45^\circ$. We adopt this from now on.

Figure 1 shows different cuts on the energy surface, for the BIA regime and σ^+ polarization, calculated for a fixed value of $k_{\parallel} = 3$, and different values of φ when a uniform field, $F_0 = 5$, is applied. For InSb¹² and the given F_0 , the critical values are $\varphi_c^+ = 34.842^\circ$ and $k_{\parallel}^c = 1.768$. The panel for $\varphi = 0$ shows the non-parabolic spin-splitted dispersions for *spin-up* and *spin-down* branches. For a given energy inside the gap region, the *spin-up* states have imaginary values for k_z along a *real line*, shown as dotted green lines in the panel with $\varphi = 90^\circ$, and these states do not propagate. The next panel with $\varphi = \varphi_c^+$ shows the situation where $E_g(k_{\parallel}, \varphi_c^+, k_z = 0) = 0$. Just above this angle, at $\varphi = 35^\circ$, the gap opens again and an *inverted* group-velocity layer of *spin-up* states (inside dotted blue-box) appears between critical k_z -values, $\pm k_{c1}$, where the z -group-velocity vanishes. The existence of this branch is

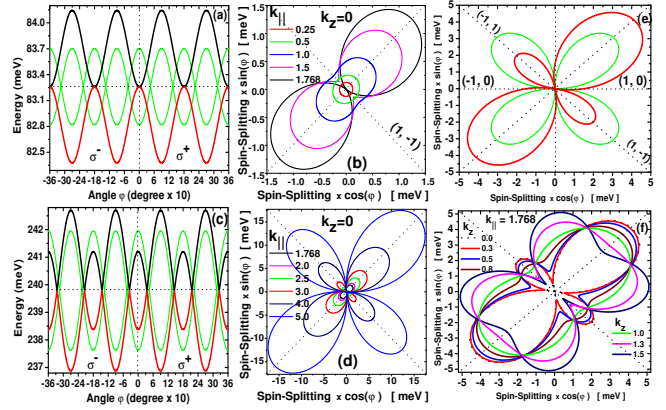


FIG. 2: Spin-splitting anisotropy for *SIA regime* (at $k_{\parallel} = 1.768 = k_{\parallel}^c$, panel *a*) and *BIA regime* (at $k_{\parallel} = 3 > k_{\parallel}^c$, panel *c*) produced by full SO (black/red lines) and BIA terms only (green lines) in bulk InSb. Panels *b* and *d*: Twofold and four-fold symmetries for spin-splitting gap in the *SIA* (*b*) and *BIA* (*d*) regimes, at different values of k_{\parallel} . Panel *e*: Comparison between Rashba and Dresselhaus interactions, for panel *c* conditions; red (green) lines for BIA+SIA (BIA) terms. Panel *f*: Spin-splitting anisotropy of σ^+ energy surfaces, away from zone-center.

determined partly by the quadratic $\alpha_2(k_{\parallel}, \varphi)$ BIA term in Eq. 1. For k_z in the vicinity of these critical points we have $E_{\pm}(\mathbf{k}_{\parallel}, k_z) \sim E_0 + S_0(k_z \pm k_{c1})^2$, with E_0 and S_0 constants. Inside the dotted blue box the state has *inverted* group-velocity and negative effective mass, such that a carrier will travel to $\mp z$ -axis for $\pm k_z$ values of the propagating wave vector. In the higher *spin-up* and *spin-down* branches outside $\pm k_{c1}$, the carriers travel with normal group-velocity. By increasing the angle to $\varphi = 45^\circ$, the double-valley region disappears, with an increasing gap that reaches its maximum value at $\varphi = 90^\circ$. The panels with $90^\circ \leq \varphi \leq 180^\circ$ just complete half of the periodicity of the σ^+ Hilbert subspaces.

The dispersions for σ^- polarization, in this BIA regime, have identical features as in Fig. 1, except that they require exchange between spin-polarizations in the sectors. The Hilbert subspaces form the degenerate Kramers doublet for circular polarizations. These σ^- and σ^+ spinors are characterized by their behavior under the time-reversal operator for zincblende symmetry, $\widehat{\mathcal{T}} = -i\widehat{\sigma}_y \widehat{\mathcal{C}} \widehat{I}$, where $-i\widehat{\sigma}_y$ flips spin and the complex conjugation (inversion) $\widehat{\mathcal{C}} (\widehat{I})$ flips momentum (position).

Figure 2a shows the angular gap variation, for both circular polarizations, at the critical situation where $k_{\parallel} = k_{\parallel}^c = 1.768$, for $F_0 = 5$. Black and red lines are the combined results for BIA+SIA terms whereas green lines show the effect of BIA terms acting alone. It becomes clear that BIA+SIA terms act in-phase and out-of-phase in each sector. This alternating change in phase between the SO Hamiltonian terms leads to a *Rashba regime* with C_{2V} symmetry, as shown in Fig. 2b for different $k_{\parallel} \leq k_{\parallel}^c$. In this regime, the Hamiltonian in Eq. 1

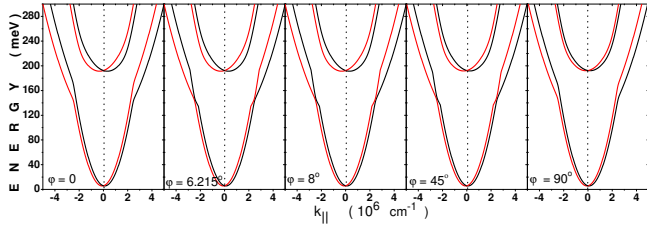


FIG. 3: 2D-subband dispersions, solutions of Eq. 1, in isolated InSb QW with $L_w = 200$ Å and uniform electric field $F_0 = 100$. Different anisotropies induced by the full SO terms result in varying in-plane masses, $m^*(k_{\parallel}, \varphi)$, and spin-splittings for each subband. Red (black) lines for down (up) spin.

produces a smooth change from s - to p -like symmetry on the electronic structure at the zone-center as k_{\parallel} increases.

Figure 2c shows the angular gap variation in the *Dresselhaus regime* (black and red lines for $k_{\parallel} = 3 > k_{\parallel}^c$, for $F_0 = 5$). The effect of BIA terms alone is shown in green lines. Here also the full SO Hamiltonian acts in-phase and the overall symmetry is changed from a twofold C_{2V} to a fourfold C_{4V} . As shown in Fig. 2d, this modification induces smooth changes on the electronic structure at the zone-center, from p - to d -like symmetry as k_{\parallel} increases. This is also at the origin of the secondary gap and the double-valley sector near the critical angle. The resulting symmetries show that it is essential to consider all the three BIA terms in the Hamiltonian, so that their cumulative effects yield the correct electronic structure and eigenstates. Observe that at given electric field there are only specific angles where the Rashba and Dresselhaus effects cancel each other.

Figure 2e compares the combined effects of BIA and SIA terms (red lines) on the spin-splitting, at the zone-center, for the same conditions shown in Fig. 2c and the red line in Fig. 2d (notice scale changing). It is clear that their effects are added along the $(\pm 1, \pm 1)$ directions of maximum spin-splitting and the BIA terms (green lines) dominate along $(\pm 1, \mp 1)$ directions where the secondary gap appears.

If we move away from the zone-center, the complexity increases. In Fig. 2f, we start with the critical situation displayed in Figs. 2a and 2b. The cuts at increasing values of k_z show new gap maxima along the $(\pm 1, 0)$ and $(0, \pm 1)$ directions. These curves are a reflection of the complex geometry of the 2D Fermi surface at different electron concentrations.

Evidence of strong anisotropy on FIR light propagating through n-type InSb bulk samples was studied by Gopalan *et al.*¹³ They have shown why the magneto-transmission experiments of Dobrowolka *et al.*¹⁴ in the Voigt and Faraday configurations, displayed maximum spin-flip and maximum transmissivity along the $(\pm 1, \pm 1)$ and $(\pm 1, \mp 1)$ directions. The electronic structure we report here arises from the same complex lattice symmetry.

Having shown the complexity of the bulk spinor environment under the full SO Hamiltonian, let us now

explore these anisotropies via the vertical transport of carriers in a DBR structure with interfaces [thickness] at positions z_{ℓ} ($\ell = 1, \dots, 4$) [$d_{\ell} = (z_{\ell+1} - z_{\ell})$] and profile $V_0(z)$. The layer $\ell = 0$ ($\ell = 4$) is the emitter (collector) contact. We use the scattering matrix technique to calculate the transmissivity and reflectivity for the system. For a given incident energy, E , we want to construct the *incoming* and *outgoing* spinor states that tunnel through the 2D states in the layer $\ell = 2$. In Fig. 3 we show 2D dispersions derived from Eq. 1, in an isolated quantum well under applied electric field. We observe that the 3D anisotropies are transferred to the subband dispersions, through anisotropic in-plane effective masses $m^*(k_{\parallel}, \varphi)$, as well as spin-splittings of each subband.

We construct each component of a spinor state, $F(\rho, \mathbf{k}_{\parallel}, z)$ in Eq. 1, as a linear combination of bulk solutions¹⁵ $\Phi(z) = \sum_{\sigma(+,-)} [a_l^{\sigma}(\mathbf{k}_{\parallel}) F_{\sigma}(+k_{z\sigma}) e^{+ik_{z\sigma}(z-z_l)} + b_l^{\sigma}(\mathbf{k}_{\parallel}) F_{\sigma}(-k_{z\sigma}) e^{-ik_{z\sigma}(z-z_l)}]$, where $a_l^{\sigma}(\mathbf{k}_{\parallel})$ ($b_l^{\sigma}(\mathbf{k}_{\parallel})$) is the amplitude of *incoming* (*outgoing*) spin-polarized waves at any given interface z_l , and $\pm k_{z\sigma}$ are real roots of $E_{\sigma}(\mathbf{k}_{\parallel}, k_z) = E$, for the carriers travelling along the z -axis. The dependence on \mathbf{k}_{\parallel} defines the open channels in phase-space. The current operator from Eq. 1 is

$$J_z(\mathbf{k}_{\parallel}, k_z) = \begin{bmatrix} J_{++} & J_{+-} \\ J_{-+} & J_{--} \end{bmatrix}, \quad (3)$$

where $J_{\sigma\sigma} = \hbar k_z/m^* + \sigma\alpha_2(k_{\parallel}, \varphi)/\hbar$ represents the spin-conserving polarized current, and $J_{+-} = -2m^*\alpha_1(k_{\parallel}, \varphi)k_z/\hbar$ the spin-flip mechanism. The vertical transport properties are also determined by the quadratic (diagonal) and linear (spin-flip) BIA SO terms. The boundary conditions require that both spinor $F(\rho, \mathbf{k}_{\parallel}, z = z_l)$ and flux $J_z F(\rho, \mathbf{k}_{\parallel}, z = z_l)$ be continuous across each interface, z_l . Resonant tunnelling for a given circular polarization implies that the matching conditions must be valid for each \mathbf{k}_{\parallel} .

The elements of the scattering matrix \mathbf{S} are the spin-conserving (t_+^+ and t_-^-) and spin-flip (t_+^- and t_-^+) transmission, and the equivalent reflection coefficients r_{\pm}^{\pm} , associated to the *incoming* and *outgoing* wave amplitudes $t_{\sigma'}^{\sigma} = a_4^{\sigma'}/a_0^{\sigma}$, for detected (σ') and incident (σ) polarizations. For any applied potential V , the partial transmissivity can be calculated¹⁵ from the ratio between detected $J_{\sigma'}^{out}$ and incident J_{σ}^{in} currents as $T_{\sigma \rightarrow \sigma'}(E, V, \mathbf{k}_{\parallel}) = \text{Re}[(t_{\sigma'}^{\sigma})^* t_{\sigma'}^{\sigma} \langle F_{\sigma'}^+ | J_{z\sigma'}^+ | F_{\sigma'}^+ \rangle_{z=z_4} / \langle F_{\sigma}^+ | J_{z\sigma}^+ | F_{\sigma}^+ \rangle_{z=z_0}]$. With the presence of spin-flip processes, the partial reflectivity is calculated from the general flux conservation, $\sum_{\sigma'} [T_{\sigma \rightarrow \sigma'}(E, V) + R_{\sigma \rightarrow \sigma'}(E, V)] = 1$, for each incident polarization. We consider vertical transport along the z -direction (001) of a symmetric InSb-InAlSb¹² DBR [$l_b = 100$ Å (barrier) and $L_w = 200$ Å (well)].

Figure 4 shows calculated partial transmissivities in the σ^+ polarization. In principle, at a given incident energy E , there will be transmissivity peaks at each spin-polarized QW level. As mentioned above, *spin-up* states cannot propagate when E is in the gap-region since the $k_{z\sigma}$ roots of $E_{\sigma}(\mathbf{k}_{\parallel}, k_z) = E$ are imaginary, as shown

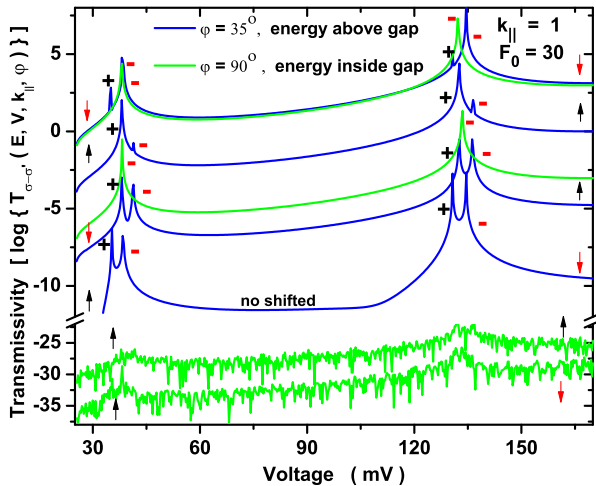


FIG. 4: Transmissivity for σ^+ spinor in InSb-InAlSb double barrier with $l_b = 100$ Å and $L_w = 200$ Å, calculated for $k_{||} = 1$, $F_0 = 30$ and $\varphi = 35^\circ$ (90°) for an incident energy above (inside) the gap, shown in blue (green) lines. The up/down arrows on left (right) indicate incidence (detection) polarizations in the DBR. Curves are shifted upwards for clarity, and small differences in peak positions of the two highest curves are due to distinct values of φ . Notice different amplitudes of each resonant peak at spin-polarized 2D levels inside QW. For energies inside the gap, only one spin propagates.

in panel $\varphi = 90^\circ$ of Fig. 1. For E outside the gap-region all polarizations propagate. The four transmissivity curves in Fig. 4 for an energy above the gap (blue lines) show double peaks at the quantum well resonances, for σ^+ -polarization. These same features occur for σ^- -polarization at equivalent angles. However, when the incident energy is inside the gap (green lines), notice that only the *spin-down* incident polarization can propagate, while the *spin-up* channels result in vanishing transmissivity. The resulting current arriving at the collector

will have Stark shifted double peaks in voltage for each quadrant.¹⁵ Since σ^+ - and σ^- -polarizations belong to orthogonal Hilbert subspaces, the vertical current produced by these states (for energies above the gap) define eight independent emitter-collector transmission channels that may be explored as voltage controlled spin-filters. In fact, polarized currents with desired polarization (\pm) can be produced with small voltage variations. Notice also that for energies inside the gap the total current is, *de facto*, *spin-down* polarized.

In conclusion we have studied how anisotropies of spinor states and dispersions of the *full* SO Hamiltonian in orthogonal Hilbert spaces, with opposite circular spin-polarized configurations, could enhance the formation of spin-filters. The possibility to tune emitter Fermi level and collector detectors requires designed magnetic contact masks on the DBR diode, a technology in full development nowadays.¹⁶ This would help exhibit and explore the complexity of the eight channels produced by the *full* SO Hamiltonian. We have shown that this new structure can work as multichannel voltage controlled spin-filters, similar to semimagnetic materials.¹⁷ We anticipate that new designed experiments will soon be able to probe the gap structure and anisotropies we predict. Finally, the possible scattering mechanisms within these two orthogonal spinor configurations must be analyzed under the unusual situation where spin and momentum coordinates are strongly coupled. Therefore, new carrier *spin-flip relaxation* times, τ_{SF} , proportional to the reciprocal of spin-splitting energy,¹⁸ $E_g^\sigma(k_{||}, \varphi_c, k_z)$, and momentum scattering times, τ_p , can be measured since $\tau_{SF}^{-1} = \tau_p \left[\frac{E_g^\sigma(k_{||}, \varphi_c, k_z)}{\hbar} \right]^2 / 2$. The very large values for $E_g^\sigma(k_{||}, \varphi_c, k_z)$ ($\sim 5 - 10$ meV) can produce devices with τ_{SF} many orders faster than τ_p .

Work is supported by FAPESP, CNPq, CAPES, US DOE grant no. DE-FG02-91ER45334, and the CMSS Program at OU.

- ¹ Semiconductor Spintronics and Quantum Computation, edited by D.D. Awschalom, D. Loss, and N. Samarth (Springer, Berlin), 2002, and references therein.
- ² S. Datta, and B. Das, *Appl. Phys. Lett.* **56**, 665 (1990).
- ³ C.F. Destefani, Sergio E. Ulloa, and G.E. Marques, *Phys. Rev. B* **69**, 125302 (2004).
- ⁴ H.C. Liu, J. Li, G.C. Aers, C.R. Leavens, M. Buchanan, and Z.R. Wasilewski, *Phys. Rev. B* **51**, 5116 (1995).
- ⁵ J. Nitta, T. Akazai, and H. Takayanagi, *Phys. Rev. Lett.* **78**, 1335 (1997).
- ⁶ G.E. Marques, and L.J. Sham, *Surf. Sci.* **113**, 131 (1982).
- ⁷ Y.A. Bychkov, and E.I. Rashba, *J. Phys. C: Solid State Phys.* **17**, 6039 (1984).
- ⁸ G. Dresselhaus, *Phys. Rev.* **100**, 580 (1955).
- ⁹ X. Cartoixà, D.Z.-Y. Ting, and Y.-C. Chang, *Appl. Phys. Lett.* **83**, 1462 (2003); J. Schliemann, J.C. Egues, and D. Loss, *Phys. Rev. Lett.* **90**, 146801 (2003).
- ¹⁰ V.I. Perel, S.A. Tarasenko, I.N. Yassievich, S.D. Ganichev,

V.V. Bel'kov, and W. Prettl, *Phys. Rev. B* **67**, 201304(R) (2003).

¹¹ E. I. Rashba, and Al. L. Efros, *Phys. Rev. Lett.* **91**, 126405 (2003).

¹² Parameters for InSb/In_{0.72}Al_{0.28}Sb: $\alpha_0 = 500$ Å²; $\beta_0 = 160$ eVÅ³; $m^* = 0.0143m_0/0.043m_0$; offset: $V_0 = 300$ meV. Units used in the paper: meV for energy, 10⁶ cm⁻¹ for wave vectors, kV/cm for electric field.

¹³ S. Gopalan, J.F. Furdyna, and S. Rodriguez, *Phys. Rev. B* **32**, 903 (1985).

¹⁴ M. Dobrowolska, Y.-F. Chen, J.F. Furdyna, and S. Rodriguez, *Phys. Rev. Lett.* **51**, 134 (1983).

¹⁵ A.C.R. Bittencourt, A.M. Cohen, and G.E. Marques, *Phys. Rev. B* **57**, 4525 (1998).

¹⁶ E.I. Rashba, *Phys. Rev. B* **62**, R16267 (2000).

¹⁷ A. Slobodskyy, C. Gould, T. Slobodskyy, C.R. Beker, G. Schmidt, and L.W. Molenkamp, *Phys. Rev. Lett.* **90**, 246601 (2003).

¹⁸ M.I. D'yakonov, and V.I. Perel, Sov. Phys. Solid State **13**, 3023 (1972).